Active coupled-resonator optical waveguides. II. Current injection InP–InGaAsP Fabry–Perot resonator arrays

Joyce K. S. Poon,* Lin Zhu, John M. Choi, Guy A. DeRose, Axel Scherer, and Amnon Yariv

Department of Electrical Engineering, California Institute of Technology, MS 136-93, Pasadena, California 91125, USA
**Corresponding author: poon@caltech.edu*

Received May 10, 2007; accepted June 4, 2007;
posted July 5, 2007 (Doc. ID 82869); published August 24, 2007

We investigate active, electrically pumped coupled-resonator optical waveguides (CROWs) in the form of InP–InGaAsP Fabry–Perot resonator arrays. We discuss the fabrication of these devices and present measurements of the transmission spectra. The signal-to-noise ratio is found to be a strong function of wavelength and degraded rapidly along the resonator chain away from the input. Our results highlight a number of ingredients toward practical implementations loss-compensated and amplifying CROWs. © 2007 Optical Society of America

OCIS codes: 230.5750, 250.5980, 140.2010.

1. INTRODUCTION

In Part I of this series of papers, we theoretically explored the effect of gain in coupled resonators [1]. In this paper, we present measurements of the transmission spectra of coupled-resonator optical waveguides (CROWs) in the form of active Fabry–Perot resonator arrays fabricated in InP–InGaAsP semiconductor materials. The gain is supplied through the injection of an electrical current. We have previously developed a theoretical model to analyze these structures using transfer matrices [2]. Our experimental results highlight a number of issues related to noise as well as device termination and excitation described in [1].

2. DEVICE FABRICATION

For practical purposes, the properties of CROWs, such as the inter-resonator coupling and optical amplification, should be electrically tunable. To this end, we fabricated CROWs in compound III-V semiconductor (InP–InGaAsP) materials. A schematic of the devices is shown in Fig. 1. Each CROW consisted of 46 laterally coupled Fabry–Perot resonators with a relatively weak index contrast of $\Delta n/n \approx 10^{-2}$ centered under a 100 μm wide electrical contact such that 25 resonators were pumped. The resonators consisted of single-mode waveguides that were 3 μm wide, and we made devices with various inter-resonator spacings near 1 μm. The resonator end mirrors were simply cleaved facets.

The devices were fabricated using a series of aligned electron-beam lithography steps using a Leica EBPG5000 system, wet chemical etching, and metal evaporation. The wafer structure is outlined in Fig. 2 with the active region consisting of four unstrained quantum wells. The wet-etch was a two step process wherein we first transferred the pattern to the thin InGaAs layer using a hydrobromic acid (HBr) etch, and then we used the InGaAs as a mask to etch the InP with hydrochloric acid (HCl). The InGaAsP acted as an etch stop for the HCl. The waveguides were aligned along the [110] direction in the InP to obtain straight side-walls. Feature sizes of the order of 100 nm can be chemically etched using this technique [3,4]. We shall briefly discuss the fabrication process, which is summarized in Fig. 3.

First, alignment markers were defined using electron-beam lithography in a 2.5 μm thick layer of polymethylmethacrylate (PMMA) (950K C10, Microchem, Newton, Massachusetts) and wet-etched into the semiconductor. We immersed the chip in a solution of HBr (48 %):HNO_3, (68%):H_2O, with a ratio of 1:1:30 for 5 s; HCl (37%):H_2O, with a ratio of 4:1 for 30 s; and $HBr:HNO_3:H_2O$, with a ratio 1:1:30 for 45 s to etch into the InGaAsP layers. The resultant markers were approximately 12 μm $\times$ 12 μm and 1 μm deep. The markers were spaced on a grid of 1.85 mm $\times$ 2.5 mm. The PMMA was stripped off using chloroform after the etching.

Subsequently, a 250 nm thick layer of PMMA (495K C4, Microchem) was spun onto the chip and an electron-beam exposure aligned to the markers was performed to define the trenches between the resonator waveguides. After the lithography, the gaps were etched by immersing the chip in $HBr:HNO_3:H_2O$, with a ratio of 1:1:30 for 5 seconds and $HCl:H_2O$, with a ratio of 4:1 for 30 seconds.

After removing the residual PMMA, a dilution of methylbutylisoketone (MIBK): flowable oxide 16 (FOx 16, Dow Corning, Midland, Michigan) with a ratio of 1:1.75 was spun onto the chip. The FOx layer filled the trenches and was about 350 nm thick over the unpatterned regions. FOx is a spin-on glass but can also be cured by electron-beam exposure [5]. A second aligned electron-beam exposure of the trenches was then performed. The chip was

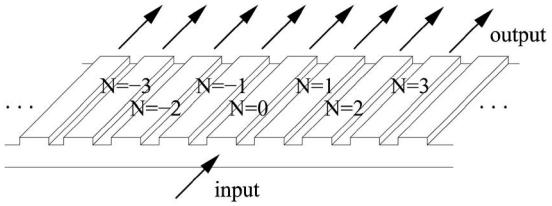

Fig. 1. Schematic of the Fabry–Perot resonator array CROW.

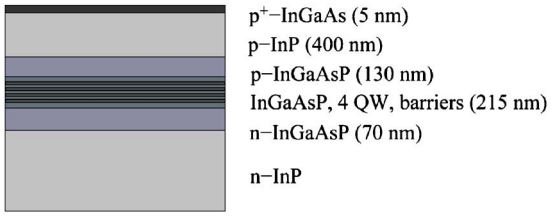

Fig. 2. (Color online) Schematic of the wafer structure.

developed in 2.4% tetramethylammonium hydroxide (TMAH) solution (CD26, Microposit, Marlborough, Massachusetts) for 30 min. The FOx patterns were wider than the trenches by 200 nm and backfilled the trenches. Without this planarization step, the devices failed to achieve laser action.

Next, electrical contacts were deposited using a lift-off process. A 2.5 μm thick layer of 1813 resist (Microposit) was spun on and exposed photolithographically. Before development in 2.4% TMAH, the chip was soaked in toluene for 1 min to create a slight undercut profile to assist the lift-off [6]. The p-side contact, Cr/AuZn/Au 2 nm/6 nm/250 nm, was deposited using a thermal evaporator. The chip was then mechanically thinned to about 100 μm thick, and the n-side contact, Cr/AuGe/Au 2 nm/6 nm/250 nm, was evaporated. Finally, devices approximately 550 μm in length were cleaved from the chip. Figure 4 shows several scanning electron microscope images of the fabricated devices.

3. MEASUREMENT

We measured the transmission spectrum at each of the coupled resonators for various injection current levels. The measurement setup is shown in Fig. 5. To measure the devices, we coupled light from a tunable laser (Agilent 81640A) from free-space to a resonator facet near the center of the device. The devices were mounted onto copper bars using an electrically and thermally conductive epoxy (H2OE-LV, Epoxy Technology, Billerica, Massachusetts), and onto a thermoelectric cooling (TEC) stage. The temperature was maintained at 20°C. We then imaged the output of the device using a high sensitivity InGaAs camera (Goodrich SU640SDV-1.7RT) to measure the transmission amplitude at each waveguide position. The waveguide positions could be readily identified from the near-field image of the device; an example is shown in Fig. 6(a). We investigated TE polarized light, which experiences more gain compared to the TM polarization [7].

The devices were pumped with current pulses with a temporal width of 200 ns and a period of 10 μs using a pulsed current source (HP 8114A). The integration time of the camera, of the order of milliseconds, was significantly longer than the pulse width and period, which automatically averaged the transmission amplitude. Laser action was observed in the devices, with a threshold peak current density around $J_{th} \approx 750\ \mathrm{A/cm^2}$, indicating that losses could be completely compensated. Figure 6(b) shows a typical light-current curve.

4. RESULTS

For the transmission measurements, we operated the devices below threshold. For comparisons with theory, we used a transfer matrix method and set the field amplification for central 25 waveguides to be 534 $\mathrm{cm^{-1}}$ to simu-

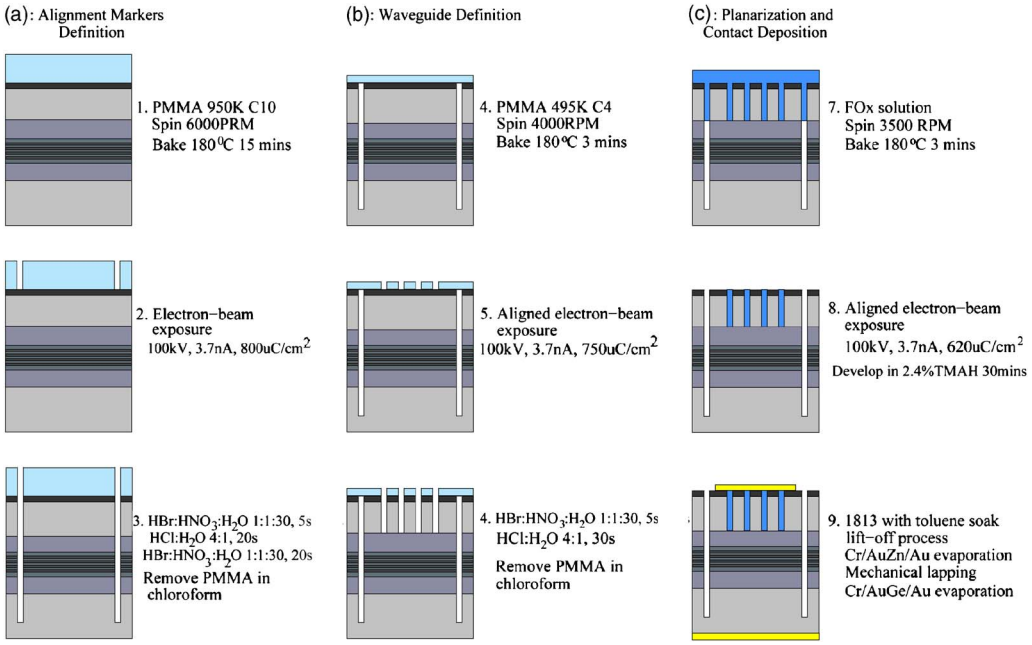

Fig. 3. (Color online) Summary of the fabrication process.

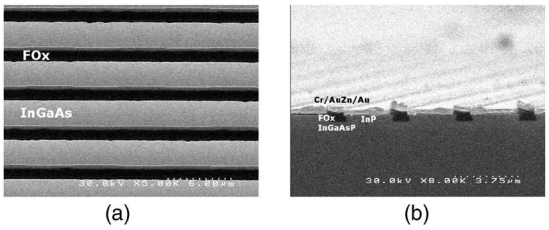

Fig. 4. Scanning electron micrographs of (a) the top view of the FOx overlay that backfilled the trenches and (b) the cross section of a completed device.

late the subthreshold regime, and the losses for the outer resonators to be 5.6 cm^{-1} to model the unpumped region [2]. The calculated normalized transmission spectra and group delay did not depend strongly on the specific value of gain we chose, as long as the calculations remained numerically stable. We did not include spontaneous emission into the transfer matrices.

Figure 7 shows the transmission spectra for two devices with inter-resonator separations of 800 and 900 nm, resulting in per length coupling constants of $\kappa_l = 1.1 \times 10^{-3}\ \mu m^{-1}$ and $\kappa_l = 0.9 \times 10^{-3}\ \mu m^{-1}$, respectively. The spatial profile of the waveguide mode was calculated with a mode-solver. The input light was focussed onto the zeroth resonator. The amplitude of the injection current was 280 mA corresponding to approximately $0.7 J_{th}$. For these plots, the spontaneous emission background in the absence of the input was subtracted from the measured amplitude. There is generally good agreement between the theoretical and experimental results. Since the spontaneous emission could be subtracted as a background, the noise was not dominated by the beating between the signal and the spontaneous emission.

Figure 8 shows the transmission spectra for the devices at various values of pump current amplitudes without subtracting the spontaneous emission background. The theoretical group delay is included as well. The dotted lines in Figs. 8(a), 8(b), 8(f), and 8(g) indicate the resonance wavelengths of a single resonator. The spectra are normalized to the maximum power at a current amplitude of 310 mA.

As evidenced by the plots, the transmission spectra vary strongly as a function of position and coupling strengths, and both peaks and notches can occur on resonance. The spectra at 280 mA are in the closest agreement with the theoretical calculations. The highest transmission amplitude does not occur at the band-edges but at the band-center even though the group delay is smaller. This can be understood from the arguments in [1] that a weak resonance is set up in the direction of periodicity be-

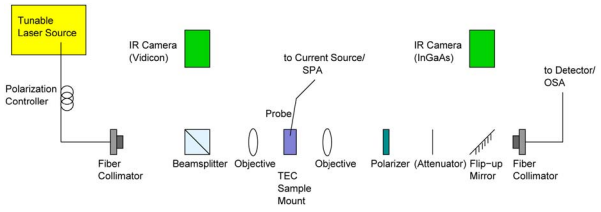

Fig. 5. (Color online) Schematic of the experimental setup. SPA is the semiconductor parameter analyzer and OSA is the optical spectrum analyzer.

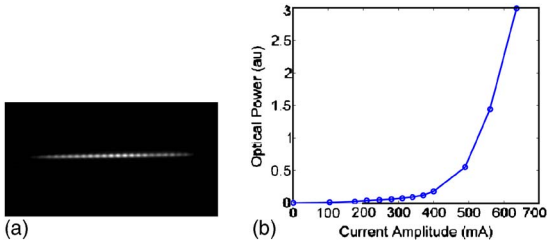

Fig. 6. (Color online) (a) Subthreshold near-field image; (b) a typical optical power versus injection current curve.

cause of the unpumped regions outside the contact, and the excitation source has varying magnitudes of spatial overlap with the modes of the structure. The group delay away from the band-center can be both positive and negative depending on the inter-resonator coupling strength. For lower loss resonators with a higher extinction ratio between the CROW band and the stop band, the anomalous group delays would occur at frequencies where the light is mostly attenuated. Because of the absorption outside the contact region, the transmission spectra do not exhibit sharp peaks.

Ideally, the transmission spectra at the various resonators should be symmetric about the excitation at $N=0$. However, the measured spectra are asymmetric, which is due to nonuniformity in the gain across the devices and the resonators. The nonuniformity can arise from the electrical contacts, slight errors in the lithographic alignment of the FOx overlay layer, as well as the gain material itself, which contributed to local bright spots in the devices.

Figure 8 suggests that the SNR degraded rapidly as a function of the resonator position. Assuming that the noise was dominated by spontaneous emission only, and not by the beating between the signal and the spontaneous emission, the measured optical power was approximately the sum of the signal and the spontaneous emission background without the input signal. Therefore,

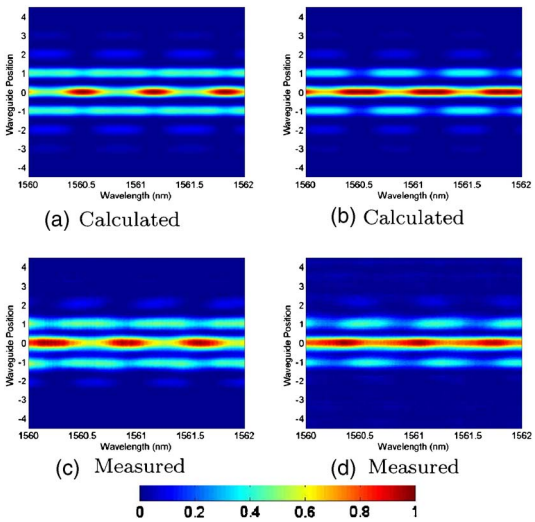

Fig. 7. (Color online) Theoretically calculated transmission spectra for (a) $\kappa_l = 1.1 \times 10^{-3}\ \mu m^{-1}$ and (b) $\kappa_l = 0.9 \times 10^{-3}\ \mu m^{-1}$, and the measured transmission spectra, less the spontaneous emission background, at a current amplitude of 280 mA for an array with inter-resonator spacings of (c) 800 nm and (d) 900 nm.

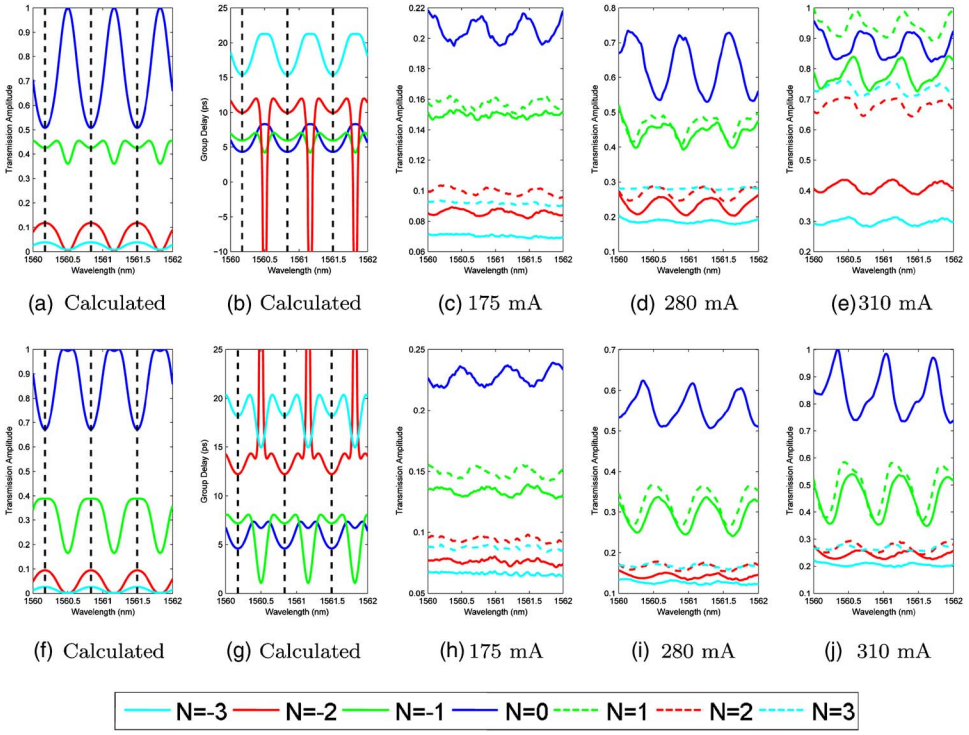

Fig. 8. (Color online) Top row: theoretical (a) transmission and (b) group delay, as well as (c)–(e) experimentally measured transmission spectra at various resonators and injection current amplitudes for an array with an inter-resonator spacing of 800 nm. Bottom row (f)–(j) the same for an array with an inter-resonator spacing of 900 nm.

$$\mathrm{SNR}_{\mathrm{opt}} = \frac{\text{Output Power with the Input}}{\text{Output Power without the Input}} - 1, \quad (1)$$

where $\mathrm{SNR}_{\mathrm{opt}}$ is the optical SNR. The electrical SNR is given by $|\mathrm{SNR}_{\mathrm{opt}}|^2$. Since we did not spectrally resolve the near-field images, the spontaneous emission power across the entire emission bandwidth of about 40 nm was collected. The noise figure can be determined by dividing the signal-to-total-source spontaneous emission ratio of the input laser source of about 27 dB by $\mathrm{SNR}_{\mathrm{opt}}$. Figure 9 shows $\mathrm{SNR}_{\mathrm{opt}}$ at an injection current of 280 mA of the resonator array with an inter-resonator spacing of 800 nm for which the transmission spectra are shown in Fig. 8(d). Because of the large measurement bandwidth, low input coupling efficiency, and the low quality factors of the resonators, $\mathrm{SNR}_{\mathrm{opt}}$ decreased to near zero after only a few resonators. Moreover, because of the resonant nature of CROWs, $\mathrm{SNR}_{\mathrm{opt}}$ depended strongly on the wavelength.

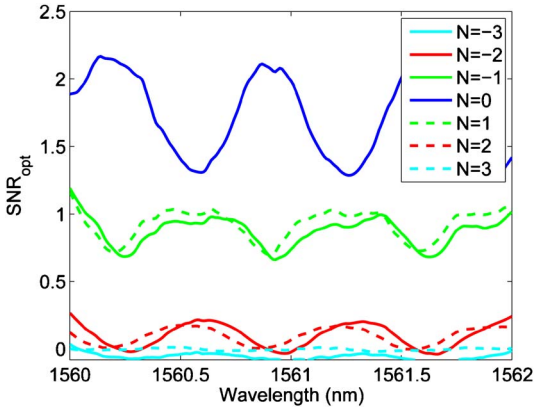

Fig. 9. (Color online) $\mathrm{SNR}_{\mathrm{opt}}$ as a function of wavelength and resonator position of an array with a transmission spectrum shown in Fig. 8(d).

5. DISCUSSION

Our demonstration represents the first steps toward realizing active CROWs, illustrating a number of technical challenges in these devices. First, because CROWs ideally consist of a very large number of resonators, the fabricated device must be uniform over its footprint. This requires uniformity in the material, etching, and electrical contacts. Second, continuous-wave (cw) operation of these devices is desirable and would enable accurate measurements of the phase response or group delay of these structures. cw operation requires improved heat dissipation that should be achievable with buried structures and improved contact resistivity.

The SNR should be increased and the noise figure should be decreased for CROWs to be practical. While the Fabry–Perot resonator arrays with cleaved facets are the simplest to implement, a relatively low facet reflectivity of ~30% implies that these resonators possess high optical losses so that a high gain is necessary. High reflectivity mirrors, in the form of gratings, for example, can be incorporated to improve the quality factors of the resonators. Asymmetric cavity designs with unequal mirror reflectivity at the two facets can reduce the amount of measured spontaneous emission noise [8]. Higher input coupling efficiency would also improve the amount of signal power coupled into the CROW to increase the SNR. This can be achieved by incorporating input and output

waveguides with mode converters much like microring CROWs or the proposed side-coupled Fabry–Perot CROWs [2,9].

Finally, since the introduction of gain allows for laser oscillation, an important question is whether CROWs should be operated above or below the laser threshold. There are benefits and disadvantages to both types of operation. Subthreshold operation is simpler to understand and model, but requires highly accurate fabrication to ensure that the resonators are identical to each other. Moreover, to suppress laser action in the CROW, the input and output coupling constants as well as the inter-resonator coupling strength should be large, which places a lower limit on the group velocity and net amplification that are attainable [1].

Operation above threshold is more complicated to analyze because locking effects may come into play, but it can be more interesting fundamentally. Above threshold, the CROW can lock to the input signal and/or the resonators can lock to each other. Phase-locked laser arrays have been studied extensively both theoretically and experimentally for several decades [7,10]. Phase-locking can occur even if the uncoupled elements are not exactly identical. The locking range, or the maximum allowed detuning for the uncoupled resonators, depends on the gain and the complex coupling coefficient between the resonators [10,11]. In general, the stronger the coupling, the larger the locking range. By increasing the optical gain, the locking range can be increased, and thus a larger variation in the uncoupled resonator resonance frequencies can be tolerated. Therefore, a light pulse centered at the laser frequency can effectively propagate through a chain of identical resonators.

On the other hand, a CROW laser can also lock to the input signal through the process of injection-locking so the input changes the operation of the CROW itself [7,12–14]. Injection-locking can be used to tune the resonance frequency of the array to or away from the central wavelength of an optical pulse to be propagated through the array. This may be a simple way to modify the dispersion of an input optical pulse to the array. Laser action can also clamp the gain, which may help in stabilizing the operation of an amplifying CROW much like gain-clamped semiconductor optical amplifiers [15–17].

6. CONCLUSIONS

In summary, we have measured the transmission spectra of electrically pumped Fabry–Perot resonator array CROWs fabricated in InP–InGaAsP. The devices could behave like lasers, indicating that losses could be completely compensated. The transmission spectra and the SNR were strongly dependent on the injection current and resonator position. The SNR of the devices degraded rapidly away from the input resonator. The devices can be improved through fabrication uniformity, lower loss resonators, and increased input coupling efficiency. We have also highlighted some possible avenues to operate laser arrays such as loss-compensated or amplifying CROWs.

ACKNOWLEDGMENTS

J. K. S. Poon thanks Will Green, Philip Chak, Andrew Stapleton, Steve Farrell, and John O'Brien for helpful discussions. She also acknowledges the support of the Natural Sciences and Engineering Research Council of Canada. The project is financially supported by the Defense Advanced Research Projects Agency (Slow Light Project) and the National Science Foundation (Award 0438038).

REFERENCES

1. J. K. S. Poon and A. Yariv, "Active coupled-resonator optical waveguides. Gain enhancement and noise," J. Opt. Soc. Am. B **24**, 2378–2388 (2007).
2. J. K. S. Poon, P. Chak, J. M. Choi, and A. Yariv, "Slowing light with Fabry–Perot resonator arrays," J. Opt. Soc. Am. B, submitted for publication.
3. K. L. Koch, P. J. Corvini, and W. T. Tsang, "Anisotropically etched deep gratings for InP/InGaAsP optical devices," J. Appl. Phys. **62**, 3461–3463 (1987).
4. E. Inamura, Y. Miyamoto, S. Tamura, T. Takasugi, and K. Furuya, "Wet chemical etching for ultrafine periodic structure: rectangular InP corrugations of 70 nm pitch and 100 nm pitch depth," Jpn. J. Appl. Phys., Part 1 **28**, 2193–2196 (1989).
5. H. Namatsu, Y. Takahashi, K. Yamazaki, T. Yamaguchi, M. Nagase, and K. Kurihara, "Three-dimensional siloxane resist for the formation of nanopatterns with minimum linewidth fluctuations," J. Vac. Sci. Technol. B **16**, 69–76 (1998).
6. M. Hatzakis, B. J. Canavello, and J. M. Shaw, "Single-step optical lift-off process," IBM J. Res. Dev. **24**, 452–460 (1980).
7. W. W. Chow, S. W. Koch, and M. Sargent III, *Semiconductor-Laser Physics* (Springer, 1997).
8. T. Mukai and Y. Yamamoto, "Noise in an AlGaAs semiconductor-laser amplifier," IEEE J. Quantum Electron. **18**, 564–575 (1982).
9. J. K. S. Poon, J. Scheuer, S. Mookherjea, G. T. Paloczi, Y. Huang, and A. Yariv, "Matrix analysis of microring coupled-resonator optical waveguides," Opt. Express **12**, 90–103 (2004).
10. D. Botez and D. R. Scifres, *Diode Laser Arrays* (Cambridge U. Press, 1994).
11. H. G. Winful, S. Allen, and L. Rahman, "Validity of the coupled-oscillator model for laser-array dynamics," Opt. Lett. **18**, 1810–1812 (1993).
12. A. E. Siegman, *Lasers* (University Science Books, 1986).
13. L. Goldberg, H. F. Taylor, J. F. Weller, and D. R. Scifres, "Injection locking of coupled-stripe diode laser arrays," Appl. Phys. Lett. **46**, 236–238 (1985).
14. J. P. Hohimer, A. Owyoung, and G. R. Hadley, "Single-channel injection locking of a diode-laser array with a cw dye laser," Appl. Phys. Lett. **47**, 1244–1246 (1985).
15. B. Bauer, F. Henry, and R. Schimpe, "Gain stabilization of a semiconductor optical amplifier by distributed feedback," IEEE Photon. Technol. Lett. **6**, 182–185 (1994).
16. L. F. Tiemeijer, P. J. A. Thijs, T. Dongen, J. J. M. Binsma, E. J. Jansen, and H. R. J. R. Vanhelleputte, "Reduced intermodulation distortion in 1300 nm gain-clamped MQW laser amplifiers," IEEE Photon. Technol. Lett. **7**, 284–286 (1995).
17. M. Bachmann, P. Doussiere, J. Y. Emery, R. NGo, F. Pommereau, L. Goldstein, G. Soulage, and A. Jourdan, "Polarisation-insensitive clamped-gain SOA with integrated spot-size convertor and DBR gratings for WDM applications at 1.55 μm wavelength," Electron. Lett. **32**, 2076–2078 (1996).